Emission Spectroscopic Studies of Plasma-Induced NO Decomposition and Water Splitting

Jian Luo,[†] Steven L. Suib,*[,†,‡] Yuji Hayashi,[§] and Hiroshige Matsumoto[||]

U-60, Department of Chemistry, University of Connecticut, Storrs, Connecticut 06269-3060, Department of Chemical Engineering and Institute of Materials Science, University of Connecticut, Storrs, Connecticut 06269-3060, Fujitsu Laboratories, Ltd., 1015 Kamikodanaka, Nakahara 211, Japan, and Department of Chemistry, Nagasaki University, Bunkyomachi 1-14 Nagasaki 852, Japan

Received: March 22, 1999; In Final Form: May 27, 1999

NO decomposition and water splitting with ac (alternating current) power plasmas at atmospheric pressure have been studied using both quartz and metal reactors. Optical emission spectroscopic (OES) studies have been carried out by employing a CCD (charge-coupled device) detector to monitor the change of plasma species neat and in the presence of reactants and metal surfaces to provide mechanistic information. Selective features of energy transfer from excited helium species to reactant molecules have been observed. Energy transfer in nitrogen plasmas is nonselective, whereas in argon plasmas it is slightly selective. Energy efficiency of plasma-induced reactions is largely determined by the efficiency of energy transfer and catalytic effects of metal surfaces. A mechanism has been proposed on the basis of OES and activity data that comprise energy transfer from excited carrier gas species to reactant molecules and heterogeneous catalysis of metal electrodes involving adsorption and combination of intermediates (oxygen radicals) on metal surfaces.

I. Introduction

Plasma methods have been extensively used in materials processing and the abatement of air pollutants such as halogenated hydrocarbons, NO_x, and SO_x.[1−11] Other plasma research areas include ozone formation, ammonia synthesis, and activation of CH_4, H_2O, and CO_2.[12−21] Many types of plasmas, such as radio frequency (rf), microwave (MW), direct current (dc), and alternating current (ac) plasmas, have been used for these purposes. Virtually any reaction may be initiated by plasmas; however, the applications of plasmas are often limited by such factors as low output due to operation at low pressures as in the case of rf/MW plasmas. Alternating current plasmas have been shown to be very efficient in employing electrical energy for excitation of gaseous molecules (thus activating reactants) at atmospheric pressure and low temperatures without sputtering of metal electrodes, which is generally unavoidable with dc plasmas. High output with high-energy efficiency is possible. Therefore, ac plasma induced reactions have aroused extensive recent attention.[22−25]

In recent years, we have used ac plasmas to activate small molecules such as NO_x (NO and NO_2), CO_x (CO and CO_2), H_2O, and CH_4. Research documenting the influence of operational parameters, types of plasma reactor, and kinetics studies in certain processes such as NO_x decomposition has been published.[22−25] In these reactions, different metal electrodes usually result in a significant difference in performance, which is ascribed to different catalytic functions. However, there have long been disputes over the role of metal electrodes in plasma-induced reactions as to whether metal electrodes are simply conductors of electricity or also catalytic.[17,21,26−28] To demonstrate the catalytic effects of metal surfaces, the roles of plasmas (as energy providers) and surfaces of metal electrodes (as possible catalytic sites) need to be investigated separately.

Another most frequently encountered concern is the effect of energy. How is energy transferred from plasma media to reactant molecules? How is the energy efficiency of a reaction determined by energy-transfer processes? How are energy-transfer processes influenced by diluent gases? These are important questions that need to be answered in order to more fully understand plasma-induced reactions.

The focus of this study is to investigate energy-transfer processes in plasmas and the effects of metal surfaces in plasma-induced reactions. A quartz reactor and several metal electrodes are employed in NO decomposition and water splitting with low-temperature ac plasmas. The use of a quartz reactor makes it possible to conveniently investigate plasma-induced reactions in the absence of metals and to distinguish the effects of plasmas and metal electrodes. The reaction intermediates and interactions between species in the plasma and metal surfaces are studied by monitoring emission spectra using a charge-coupled device detector.

II. Experimental Section

A. Plasma Reactors and Related Apparatus. Metal rods as electrodes were obtained from Enthone-OMI, Inc. of New Haven, CT. A plasma reactor consists of a stainless steel rod coated (2 μm thick) with a specific metal anode (8.0 mm in diameter) and an encircling quartz tube (9.5 mm i.d.), wrapped around by an aluminum foil (60 mm wide) serving as a cathode (Figure 1). Reactants flow through the gap between the metal rod and the quartz tubing. In a quartz reactor a stainless steel rod of 7 mm is inserted into a quartz tube (8.0 mm i.d.) and only acts as an electrode, where reactants do not make contact with any metal parts. This feature of quartz reactors makes it possible to independently study the role of plasmas in these reactions, without the participation of metal surfaces.

* To whom correspondence should be addressed.
[†] Department of Chemistry, University of Connecticut.
[‡] Department of Chemical Engineering and Institute of Materials Science, University of Connecticut.
[§] Fujitsu Laboratories.
[||] Nagasaki University.

10.1021/jp990974h CCC: $18.00
Published on Web 07/16/1999

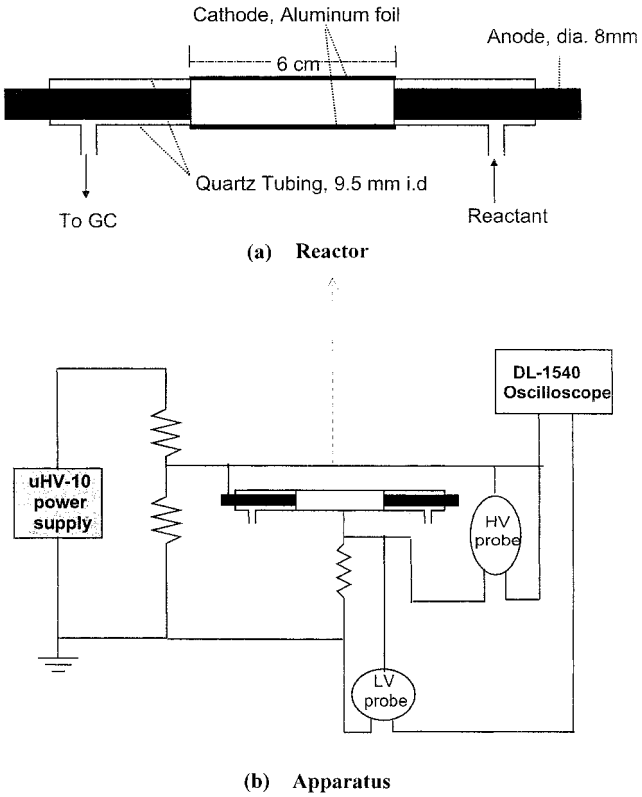

Figure 1. Structure of tubular plasma reactor (a) and related apparatus (b) for generation of plasma and determination of plasma parameters.

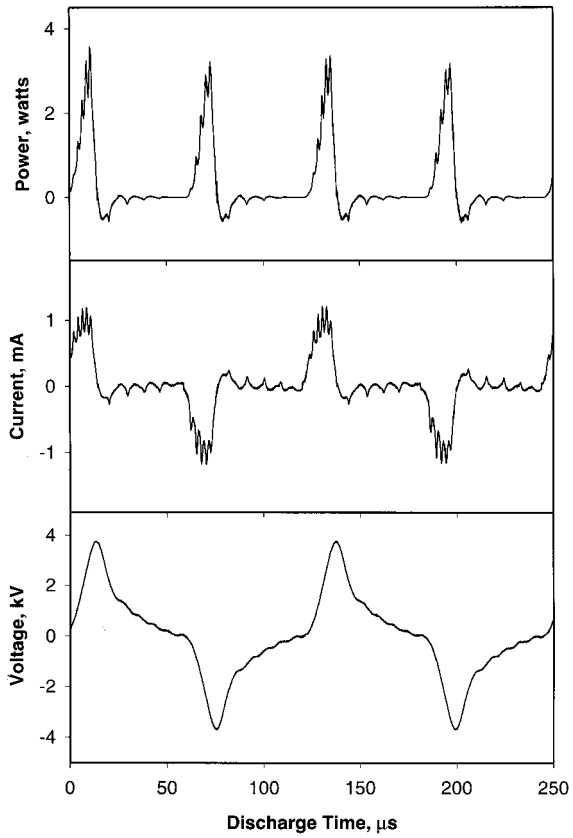

Figure 2. Waveform showing peak-to-peak voltage, current, and power of plasmas.

Figure 1b shows a diagram of the apparatus. High voltage for generating plasmas is provided by an UHV-10 ac (8.1 kHz) power supply (Nihon Inter Electronics Corporation, Japan). The current, voltage, and power during reactions are recorded as their waveforms (Figure 2), as monitored with a DL-1540 Yokogawa oscilloscope (Yokogawa Electric Corporation, Japan). A Tektronix P6025 A high-voltage probe is used to determine the voltages of the reactor, and a Yokogawa 70996 low-voltage probe is used to determine the current. After the resistance of the reactor is determined, the power is calibrated to give the energy consumption of the reaction, referred to as plasma power.[22] Slight drifts (<5%) in waveforms were sometimes observed; however, no significant change in activity corresponding to the drifts was observed.

Certified gas mixtures of 0.45% and 1.0% NO in He were obtained from MG Industrial Gas Products, Inc. Reactants of lower concentrations were made with a gas-mixing panel. Helium was used as a carrier gas to transport water vapor from a bubbler to the reactor. By adjustment of the ambient temperature or addition of a diluent gas, the concentration of water can be varied in the range 0.2−5%. When higher concentrations of water are needed, the whole system of bubbler, reactor, and connecting lines is put in an oven set at the proper temperature. Analyses are usually done on-line with an HP-5990A gas chromatograph (GC) equipped with a TCD (thermal conductivity detector) and a Carboxcen column. An MKS-UTI PPT quadrupole mass spectrometer (Q-MS) is used to detect NO_2, N_2O, N_2O_3 (and other N_xO_y species), and ozone, which may be byproducts. N_2/O_2 are the main products, with small amounts of NO_2 and N_2O detected by Q-MS. Almost no other N_xO_y species or O_3 are detected ($<10^{-14}$ Torr).

B. Emission Spectra, Plasma Excitation Temperatures, and Real Gas Temperatures. Emission spectra of the plasmas were monitored in the range 200−900 nm with a 270 M Spex liquid-nitrogen-cooled CCD detector. Spectra of helium of ultrahigh purity (99.999%) were initially taken to determine the excitation temperature (T_{exc}, close to electron temperatures for near-atmospheric pressure plasmas) using the Boltzmann plotting method.[24,29,30] T_{exc} is obtained from the slope of the plot of $\ln[I\lambda/(g_iA_{ij})]$ vs E_i (inset in Figure 3b) as given in

$$T_{exc} = 1/(k \times \text{slope}) = 1/(0.695 \times \text{slope}) \qquad (1)$$

where I is the intensity of the He atom line at wavelength λ, g_i is the statistical weight of the level, A_{ij} is the transition probability, E_i is the excitation energy of the emitting level, and k is the Boltzmann constant, 0.695 cm^{-1} K^{-1} (more commonly 8.314 J mol^{-1} K^{-1}). The excitation temperature increases with increasing input voltage in the range 2500−4500 K (Figure 3). Reactants were then used for spectroscopic studies. Experimental conditions are identical to those described above except that several holes (2 mm in diameter) are made in the aluminum foil to let the light from plasmas be collected and directed to the monochromator through a fiber optic. Relative errors in determining peak areas are within 2%.

A thermometer is attached to the aluminum foil to estimate the real gas temperatures, which are also characteristic parameters of the plasma. The gas temperature was observed to be below 40 °C at different input voltages. This demonstrates that the reactions are low-temperature plasma-induced processes instead of thermal reactions induced by high temperatures.

C. Definitions and Calculations. The free space between the aluminum foil and metal electrode is defined as plasma space (V_{plasma}, 1.24 mL). The void volume of the reactor and line is ca. 5 mL. A fluid of gas passes through it like a piston flow, quickly reaching a steady state (<0.3 min at a flow rate of 20 mL/min). This permits rapid, prompt monitoring of the changes in concentration.

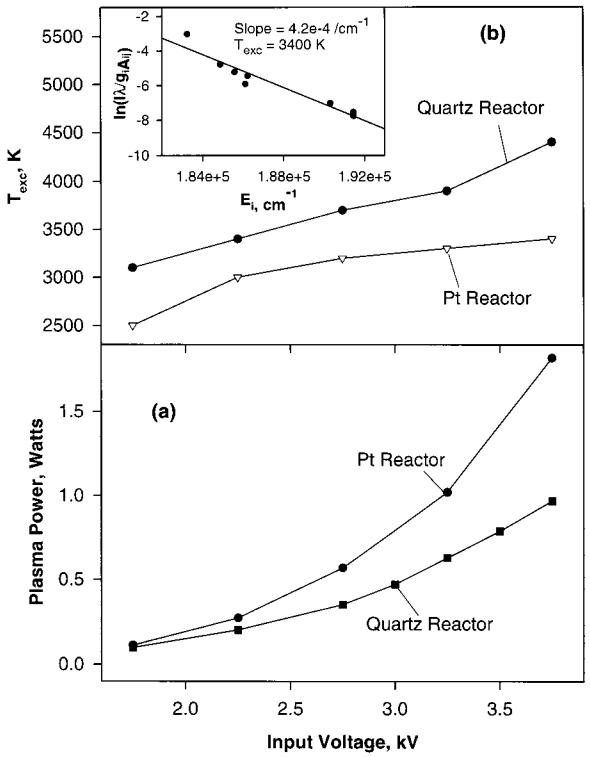

Figure 3. Dependence of plasma power (a) and temperature of excitation (b) with input voltage. The inset shows how to obtain T_{exc} from Boltzmann plotting (quartz reactor, 2.25 kV, 20 mL/min He), where I is the integrated intensity at wavelength λ, g_i is the weight of the level, A_{ij} is the transition probability, and E_i is the excitation energy of the emitting energy. The data of g_i, A_{ij}, and E_i are obtained from ref 29.

Conversions of NO (χ) are calculated from the concentrations of NO before ($[NO]_0$) and after ([NO]) reaction, as given by eq 2:

$$\chi, \% = (1 - [NO]_0/[NO]) \times 100\% \quad (2)$$

Hydrogen yields (Y_H) are calculated from concentrations of hydrogen (C_H) and water (C_W) as given in eq 3:

$$Y_H = (C_H/C_W) \times 100\% \quad (3)$$

Since water decomposition is the only detected gas-phase reaction in the system, hydrogen yield is equal to water conversion. These two concepts are hereafter used synonymously.

For NO decomposition, specific energy consumption (kilojoules per mole of converted NO, kJ/(mol NO)) is used to represent the energy efficiency of the reaction. For water splitting, energy efficiency is calculated from the hydrogen concentration ($[H_2]$, in vol %), flow rate (Q, in mL/s), power calibrated for the reaction (P_r, in watts or J/s), and free energy change for water decomposition ($\Delta G° = 229 \times 10^3$ J/mol for $H_2O \rightarrow H_2 + {}^1/_2O_2$) as given in eq 4:

$$E = 0.93\frac{\Delta G° Q[H_2]/22400}{P_r} \times 100\% \quad (4)$$

where 0.93 is a temperature calibration factor and Q is the flow rate of the reactant.

Energy-transfer efficiency is used in our emission spectroscopic studies. The intensity of an emission line relative to the highest emission line (706.4 nm for helium plasmas, 763.5 nm for argon plasmas, and 337.1 nm for nitrogen plasmas) is referred to as relative intensity of the line. The percent decrease in the intensity of any emission line at the addition of reactant is defined as the energy-transfer efficiency of the emitting state. The one corresponding to the emitting state of the basal emission line is used to represent the energy-transfer efficiency of the reaction.

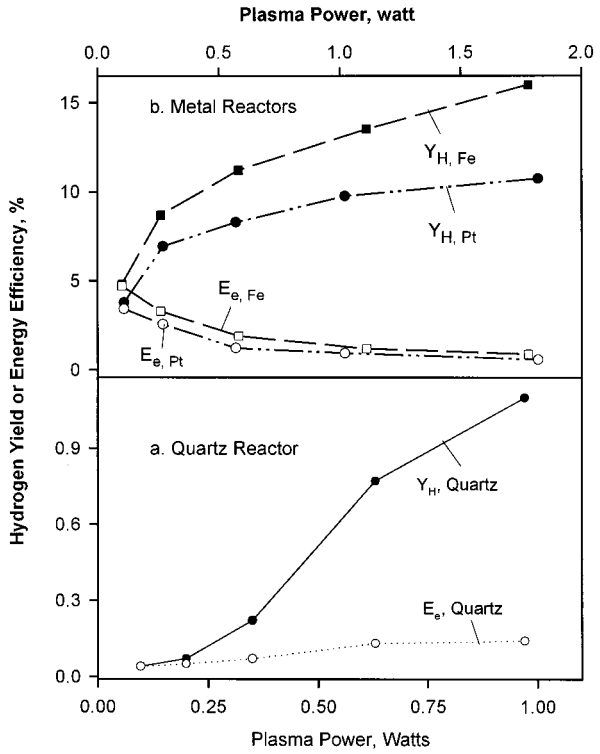

Figure 4. Variation of activity of (a) NO decomposition and (b) water splitting with time on stream in various plasma reactors.

III. Results

A. Plasma-Induced Reactions with Different Types of Reactors. *1. NO Decomposition.* NO of 250−10000 ppm can be effectively decomposed into N_2/O_2, which are the main products at all voltages (1.75−4.25 kV, corresponding plasma power of 0.1−2 W). At higher NO concentrations (>4500 ppm), NO_2 may also be an important product when the conversion is <40%. When the input voltage is increased, both the plasma power and temperature of excitation of the plasma increases (Figure 3). NO conversion increases as input voltage is increased and as flow rate and initial concentration of NO are decreased. For metal reactors, the activity follows a sequence of Rh > Cu > Pt > Fe, with a sequence of deactivation rate of Fe > Cu > Pt > Rh (1.0% NO, 3.25 kV, 45 mL/min; Figure 4a). The energy efficiency is ca. 3×10^3 to 2×10^4 kJ/(mol NO), which is smaller than that reported for NO decomposition with electron beam plasmas and much higher than that with corona glow discharge plasmas.[4] Lower but stable activity is obtained with the quartz reactor. No significant deactivation was observed with a quartz reactor even after a time on stream of 2 weeks. Detailed variation of NO conversion with input voltage, plasma energy, flow rate, etc., was reported in previous work.[22]

2. Water Splitting. Water splitting is done at 1.75−3.75 kV, C_W of 1.5−10%, and flow rate of 5−150 mL/min. Figure 4b shows the results at 3.25 kV, C_W of 3.1%, and 20 mL/min. The yield of hydrogen with a quartz reactor is only 1.0% at $t = 2$

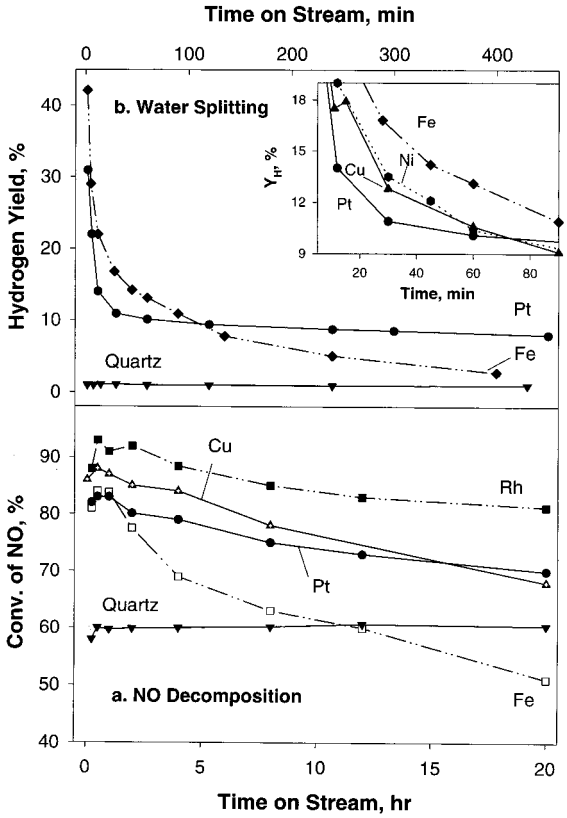

Figure 5. Dependence of hydrogen yield and energy efficiency on plasma power for quartz (a) and metal (b) reactors in water splitting (3.1% H_2O/He, 20 mL/min).

min, with an energy efficiency of 0.014%. No deactivation was observed in the following 20 h. At $[H_2O]_0$ of 5%, 4.25 kV, and 20 mL/min, the energy efficiency for a quartz reactor was 0.4%. A Pt reactor shows a much higher initial activity but considerable deactivation. Other metal reactors also show much higher initial activities than the quartz reactor, with a sequence of activity of Fe > Ni ~ Cu > Pt ≫ quartz. The activity and energy efficiency with metal reactors are much larger than those with quartz reactors, irrespective of input voltage or plasma energy. Figure 5 shows the yield of hydrogen and energy efficiency as a function of the plasma power deposited into the reactant. The energy efficiencies for metal reactors are generally 2−11% in our studies. In photocatalytic water splitting with visible light, the quantum efficiency is ca. 0.3%,[31−33] which is comparable to our results for water splitting with a quartz reactor but much smaller than those of a metal reactor. However, the energy efficiency for water electrolysis is ca. 45−60%,[34] much larger than our results (11% at 2.25 kV, 20 mL/min of 7% H_2O/He) of plasma-induced water splitting.

For a quartz reactor, the molar ratio of O_2 to H_2 product at $t = 2$ min and afterward is 0.5, equal to that of stoichiometric water decomposition. For a metal reactor, the ratio is almost zero at $t = 2$ min and increases with time, gradually reaching 0.5 for Rh and Pt reactors or a little less than 0.5 for Ni and Fe reactors in less than 30 min. The initial stage of oxygen loss shows that oxygen from water splitting was partially consumed by fresh metal electrodes. After reaction (2 days, either NO decomposition or water splitting), the surface of the quartz reactor remains the same. This accounts for the very good stability. The shiny surfaces of Pt and Rh electrodes become dull, while layers of black powder may be observed on the surfaces of Fe and Ni electrodes (green powder on a Cu electrode). No further oxygen loss was observed with stable metal electrodes such as Rh and Pt. However, active metal (Fe, Ni, Cu) electrodes react with some oxygen ($<^1/_{10}$, as deduced from analysis data) formed in plasma-induced reactions after the initial oxygen loss.

The diluent gas also makes a difference. Under the same conditions, helium plasmas produce the highest hydrogen yield, followed by argon plasmas, corresponding to much higher hydrogen yield than with nitrogen plasmas. At 2.75 kV, 20 mL/min, and concentration of water of 3.1%, the hydrogen yield with different plasmas exhibits a sequence of He (8.25%) > Ar (6.9%) > N_2 (2.0%). The sequence of energy efficiency is He (2.0%) > Ar (1.2%) > N_2 (0.7%).

B. Mechanistic Studies of the Plasma-Induced Reactions. *1. Energy Transfer from Excited Carrier Gas Species to*

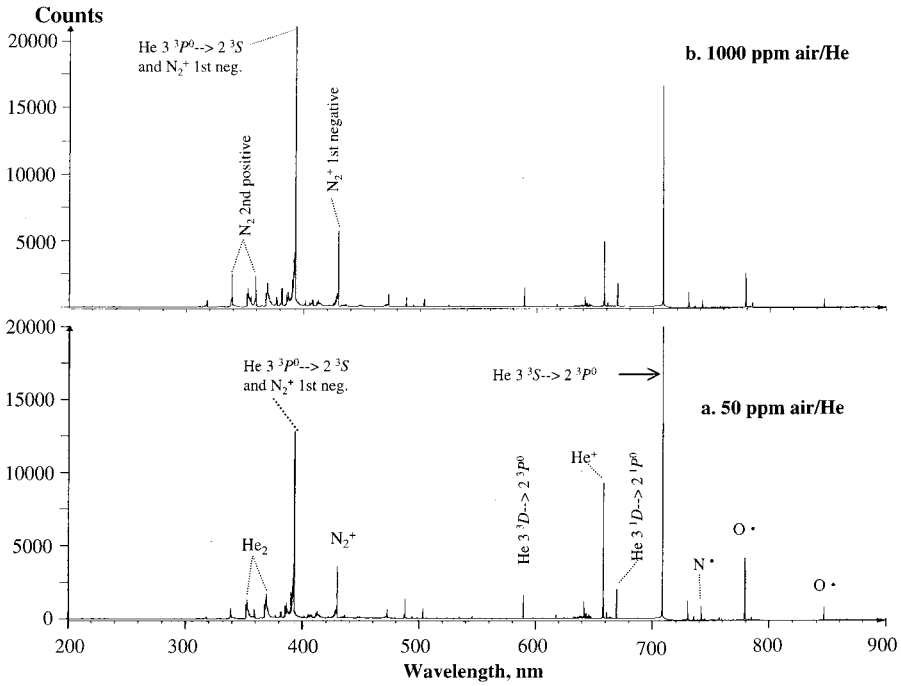

Figure 6. Emission spectra of plasmas of 50 ppm air/He (a) and 1000 ppm air/He (b) with quartz reactors (4.2 kV, 20 mL/min).

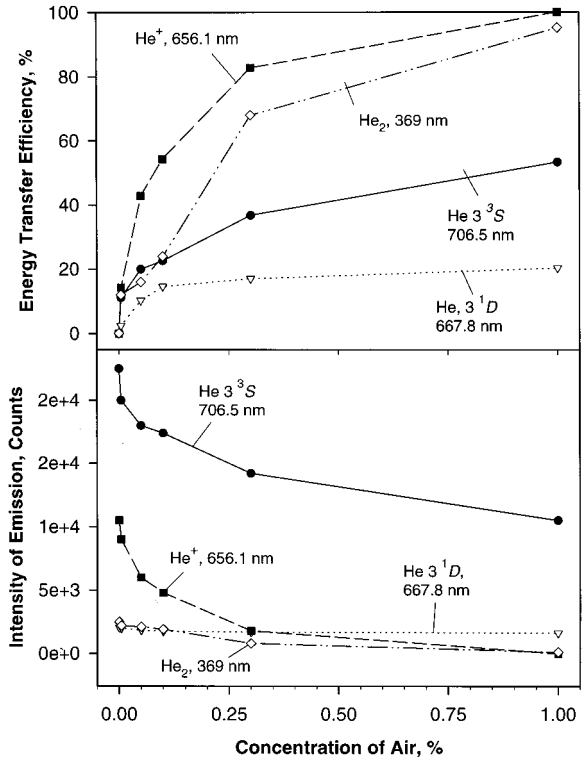

Figure 7. Variations of intensities of important excited helium plasma species (He^+, 656.1 nm; He_2, 369 nm; He 3^3S, 706.5 nm, He 3^1D, 667.8 nm) (a) and corresponding energy efficiencies (b) with concentration of air.

Reactant Molecules. Gaseous molecules other than carrier gas in the plasma reactions are NO, N_2/O_2, and H_2O. The influence of addition of these gases on plasmas was examined with emission spectroscopy. Different gases (air, NO, and H_2O) with different concentrations (50 ppm, 5%) were used to investigate energy-transfer processes in plasmas.

a. Energy Transfer from Excited He Series Species to Different Gaseous Reactants. Emission lines of the helium series including He (whose basal line is at 706.5 nm, with other important lines at 388.9 and 667.8 nm, etc.),[35] He^+ (656.1 nm),[35] He_2 (ca. 368 nm),[36] and He_2^+ (ca. 600 nm)[37,38] are observed in the spectra of helium of ultrahigh purity (99.999%). The intensities of all these emissions increase when the input voltage is increased. When 50 ppm of air is introduced, intense emission of N_2^+ first negative system ($B^2\Sigma_u^+ \rightarrow X\Sigma_g^+$ transitions at 388−391 and 425−428 nm)[41] and small signals of N_2 second positive system ($C^3\Pi_u \rightarrow B^3\Pi_g$ transitions at ca. 337.1 and 357.7 nm)[36,39−41] appear, together with strong signals of oxygen radicals at 777.4 and 844.0 nm (Figure 6). Nitrogen radicals are also observed at 746 nm. When the concentration of air is increased, the intensities of the main He series decreased considerably while those of N_2 and N_2^+ increased. At an air concentration of 1.0%, emission of He^+ and He_2^+ disappeared. The intensity of He_2 decreased by over 90%. The intensity of the basal He line (706.5 nm) decreased by ca. 50%. The variations of intensities of some typical helium species and corresponding energy efficiencies with the concentration of air are shown in Figure 7. Excited species of He^+, He_2^+, He_2, and He 3^3S changed dramatically in intensity upon addition of and with increasing air concentration. The intensities of He atoms other than He 3^3S such as those at 388.9 nm (He 3^3P^0), 587.6 nm (He 3^3D), and 667.8 nm (He 3^1D) remained relatively unchanged, indicating that the interactions between different states of helium atoms and air are of different strengths.

When NO is introduced (even at 0.1% NO), no emission lines of He^+, He_2, or He_2^+ can be observed. The intensity of He lines at 706.5 nm (corresponding to the emitting state of He 3^3S) decreased markedly, with the energy-transfer efficiencies being much larger compared to the addition of air. Little change in the intensities of other emission lines of He atoms was observed with NO added to He plasmas even at [NO] = 1.0%. High-intensity signals of N_2/O_2 (as products from decomposition of NO) are present in the plasmas. Both oxygen and nitrogen radicals of high intensities were observed (Figure 8a). The variations of intensities of some He emitting species with concentration of air are shown in Figure 9a. The energy transfer from excited He^+, He_2, He_2^+, and other He species to NO is much more efficient than that to air. In addition, the energy transfer from different excited He atoms to NO is also selective.

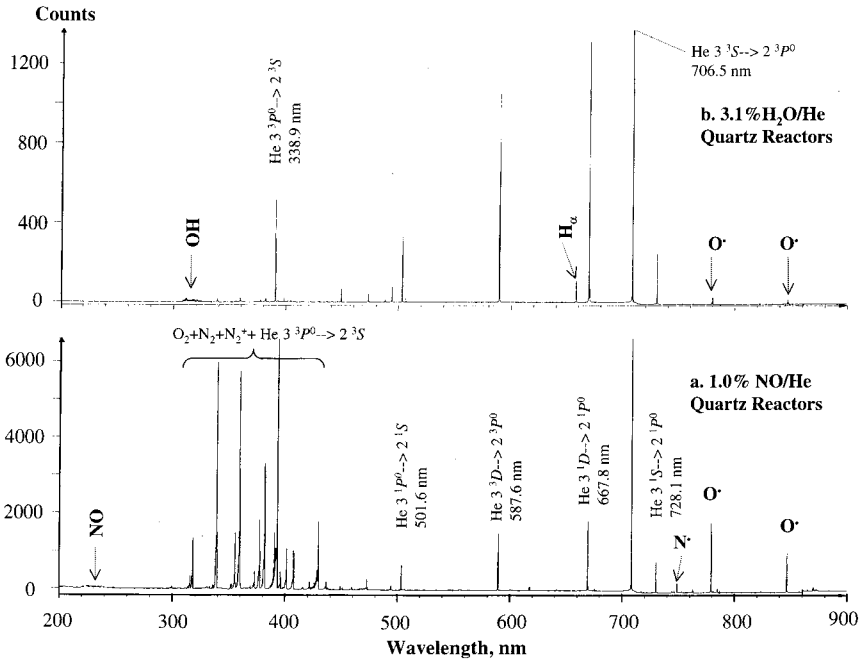

Figure 8. Emission spectra of 1% NO/He (a) and 3.1% H_2O/He (b) with quartz reactors (4.2 kV, 20 mL/min).

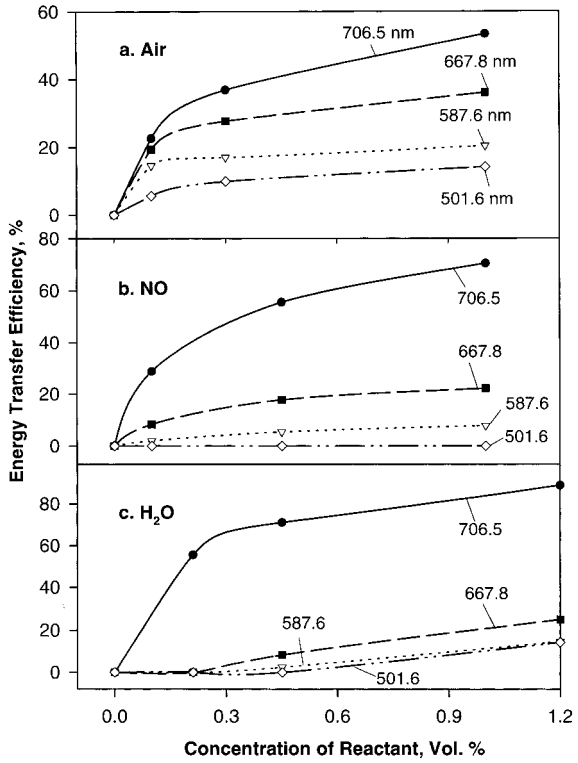

Figure 9. Variations of intensities of characteristic excited helium atoms (He 3^3S, 706.5 nm; He 3^1D, 667.8 nm; He 3^3D, 587.6 nm; He 3^1P^0, 501.6 nm) with concentration of reactant for plasmas of helium with (a) air, (b) NO, and (c) H_2O (4.2 kV, 20 mL/min).

When water (even <0.2%) is present, all emissions of He^+, He_2, and He_2^+ disappeared completely. The intensities of He emission at 706.5 nm decreased steeply by over 90% at [H_2O] = 1.2%, at which the 587.6 and 667.8 nm lines were still relatively unchanged. In some cases the 667.8 nm line became the highest-intensity emission when the concentration of water is over 3.1%. Emissions of H_α (656.2 nm) and OH radicals (306−309 nm)[42,43] were observed along with small signals of oxygen radicals at 777.2 and 844.6 nm with the addition of H_2O (Figure 8b). Figure 9c shows the variation of these species with concentration of H_2O in He plasmas with quartz reactors. Obviously, excited species of He^+, He_2, and He_2^+ can very effectively transfer energy to reactant molecules (NO, H_2O), whereas different states of excited He atoms transfer energy to reactant molecules unproportionately, or in a selective manner. In fact the energy transfer from different excited He atoms to water molecules is the highest among the reactants.

For all the three gaseous reactants, the energy-transfer efficiency increases when the concentration of reactant is increased. At the same concentration, the energy-transfer efficiency increases with increasing input voltage.

b. Energy Transfer from Different Carrier Gas to Water Molecules. In this section the energy transfer from different carrier gases (Ar and N_2) to water is examined by monitoring the intensities of characteristic emission lines of each carrier gas. The results are compared to selective features of helium plasmas (Figures 10−12).

The spectra of plasmas of N_2 are shown in Figure 10. The second positive N_2 system is the main emission, with small signals of the N_2^+ first negative system, indicating a slight ionization feature of nitrogen plasmas under our experimental conditions. With a [H_2O] < 1%, the decrease in intensities of N_2 emission is small (<20%), although a slightly larger relative decrease in the emission of N_2^+ was observed. All the emission lines decreased in intensity by 52−58% at [H_2O] = 2.3%, with similar relative decreases in intensity for different states of N_2/N_2^+ emission. This shows that the energy transfer from N_2/N_2^+ to water molecules is nonselective in this study.

Argon atoms of different states were observed in argon plasmas. Other argon species such as Ar_2 or Ar_2^+ were not detected. Ar^+ is barely observable, in accordance with the absence of species such as N_2, N_2^+, $N^\bullet$, and $O^\bullet$ when air of up to 1% was introduced into argon plasmas, since N_2^+ in N_2/Ar plasmas is diagnostic of the presence of Ar^+/Ar_2^+ via the charge-transfer reaction between Ar^+/Ar_2^+ and N_2 to form N_2^+. This indicates that under our experimental conditions argon plasmas are only slightly ionized. When water is introduced, the intensities of emission of all excited argon atoms decreased, also by different proportions. In fact, the energy transfer of argon plasmas is between that of nitrogen plasmas and helium plasmas,

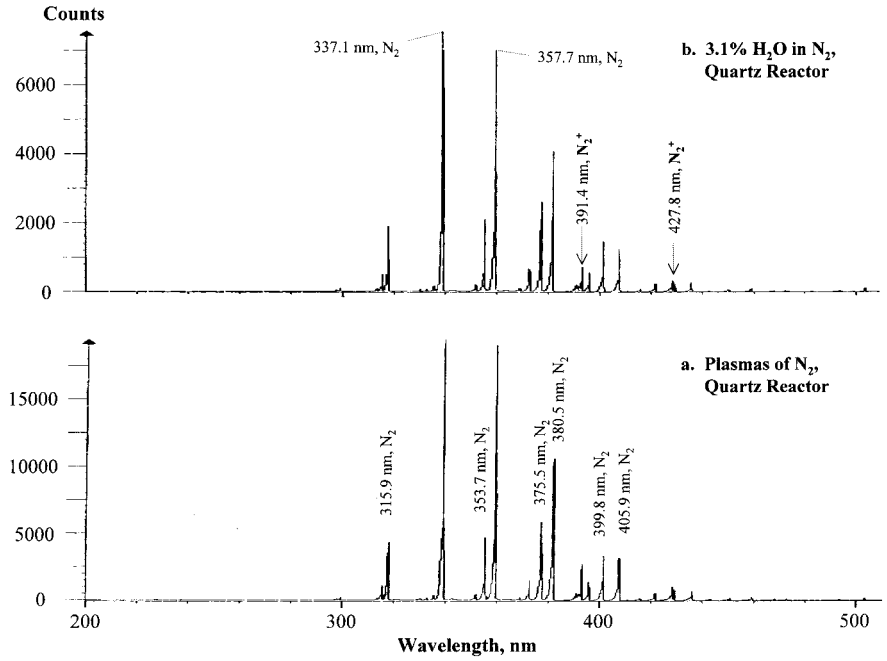

Figure 10. Emission spectra of plasmas of (a) pure nitrogen and (b) 3.1% H_2O/N_2 with quartz reactors (4.2 kV, 20 mL/min).

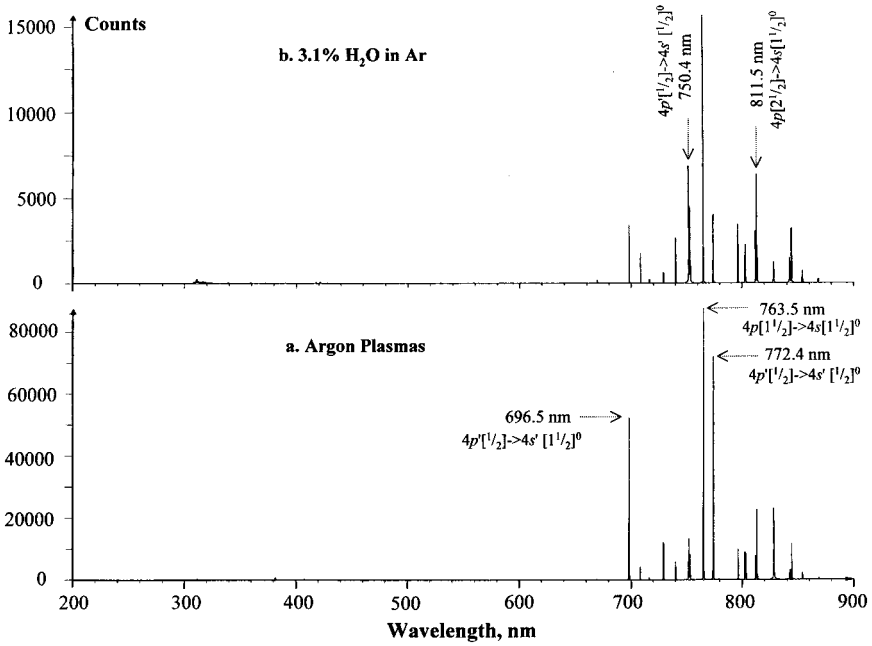

Figure 11. Emission spectra of plasmas of (a) pure argon and (b) 3.1% H_2O/He with quartz reactors (4.2 kV, 20 mL/min).

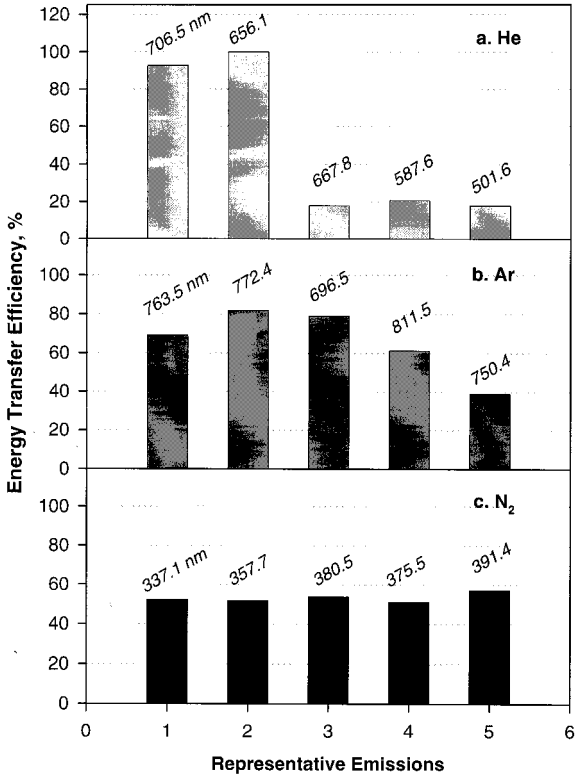

Figure 12. Energy-transfer efficiencies of typical emitting species in plasmas of (a) He, (b) Ar, and (c) N_2 showing diluent effects on selectivity of energy transfer.

corresponding to a slightly unbalanced energy transfer from excited argon atoms of different states to H_2O. In addition, the degree of decrease in argon emission due to addition of water is much smaller than that in He/H_2O plasmas but much greater than that in nitrogen plasmas at similar water concentrations (Figures 11 and 12). Hydroxyl radicals are observable in H_2O/Ar plasmas, but no H_α line has been detected. Emission of H_α has been observed in He/H_2O plasmas in this study.

c. Comparison between Metal and Quartz Reactors in Energy Transfer. Relative to quartz reactors, the emission spectra of He plasmas with metal reactors such as Pt and Fe (Figures 13 and 14) show similar emission lines with total lower intensities and different relative intensities. At the same input voltages the intensities of emission lines with metal reactors are usually about half of those of corresponding spectra with quartz reactors, although the plasma power with metal reactors is usually twice that with quartz reactors. Therefore, the intensities with metal reactors are generally $^1/_4$ of those with quartz reactors at the same plasma power. The relative intensity of He^+ is much lower with metal reactors than with quartz reactors.

When air, NO, or H_2O is introduced into helium plasmas with metal reactors, the change in emission spectra shows trends similar to those with quartz reactors. However, the decrease in intensities of characteristic emission lines with metal reactors is much smaller, usually about half that of a quartz reactor under similar conditions. This indicates that energy-transfer efficiency with metal reactors is lower than that with quartz reactors.

2. Interactions between Plasma Species and Metal Surfaces. The most pronounced difference between metal and quartz reactors lies in the presence of oxygen radicals with quartz reactors and the absence of oxygen radicals with metal reactors (Figures 13b and 14). No $O^\bullet$ can be detected in metal reactors when air of up to 0.1% is added to He, compared with a relative intensity of $O^\bullet$ of >30% with quartz reactors at all concentrations of air tested here. Similarly, almost no signals of $O^\bullet$ can be observed in plasmas of 1% NO/He with metal reactors, but $O^\bullet$ of relatively intensity of >30% is obtained with quartz reactors under similar conditions, showing that $O^\bullet$ species formed from NO decomposition are probably adsorbed by metal surfaces.

In water splitting, oxygen radicals can be observed with quartz reactors, where the intensities of oxygen radicals increase with increasing input voltage but is independent of flow rate of reactants. The intensities of $HO^\bullet$ and H_α show similar trends. However, no oxygen radicals can be observed with either Pt or Fe reactors at any voltage employed here. In addition, the intensities of $HO^\bullet$ and H_α species with metal reactors are much smaller than those with quartz reactors (Figures 4, 14, and 15), although GC analyses show that the activities of metal reactors are much higher than quartz reactors.

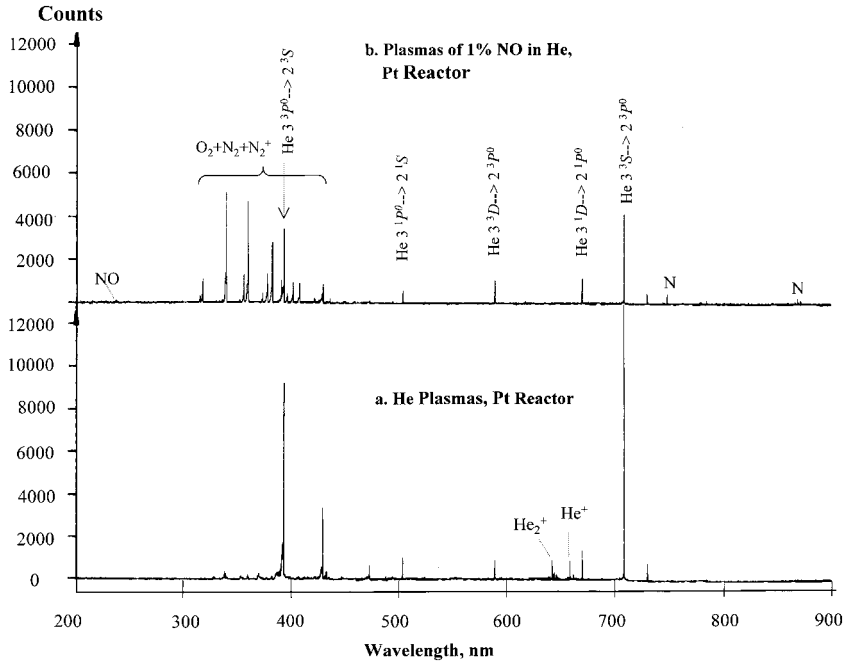

Figure 13. Emission spectra of plasmas of (a) helium and (b) 1% NO/He with Pt reactors (4.2 kV, 20 mL/min).

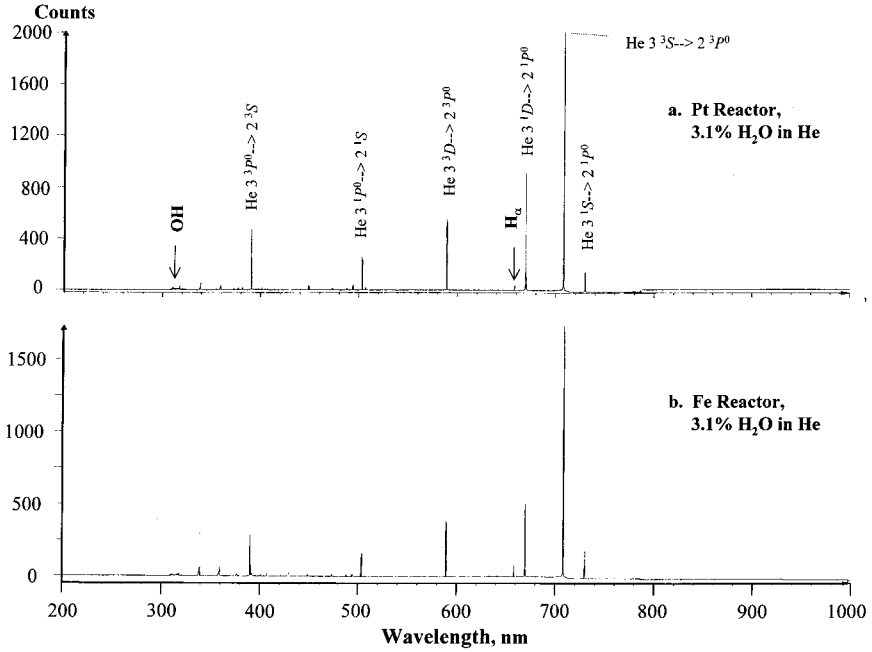

Figure 14. Emission spectra of plasmas of 3.1% H_2O with (a) Pt and (b) Fe reactors (4.2 kV, 20 mL/min).

IV. Discussion

A. Energy Transfers and Activation of Reactant Molecules. The real gas temperature of ac plasmas studied here is close to room temperature. The reactant molecules are therefore not excited by thermal energy but by high-energy electrons from the power source (direct activation), by excited plasma species of carrier gases (indirect activation), or both. The reaction data show that activity and energy efficiency both heavily depend on the type of plasma carrier gas, which almost excludes the direct activation, where activity/energy efficiency is roughly independent of carrier gas. In both plasma-induced reactions studied here, energy transfer from excited species to reactant molecules has been observed. This energy transfer should be the main pathway for activation of reactant molecules, considering that the carrier gas is the predominant component of the reaction mixture.

From the data of intensity change in air/He plasmas, the sequence of efficiency of energy transfer for different helium series species is $He^+/He_2^+ > He_2 > He\ (3^3S) \gg$ other states of excited helium atoms. Other excited helium species are almost inactive in energy transfer. Excited N_2 second positive/N_2^+ first negative systems and oxygen radicals are the main products, as well as nitrogen radicals. Similar features of energy transfer and larger efficiency in NO/He plasmas have been observed. The main products are N_2/O_2 with radicals of $N^\bullet/O^\bullet$ as intermediates. The energy transfer in H_2O/He plasmas shows similar features and the largest efficiencies. The products are H_2/O_2 with $HO^\bullet/H^\bullet/O^\bullet$ as intermediates. The main model

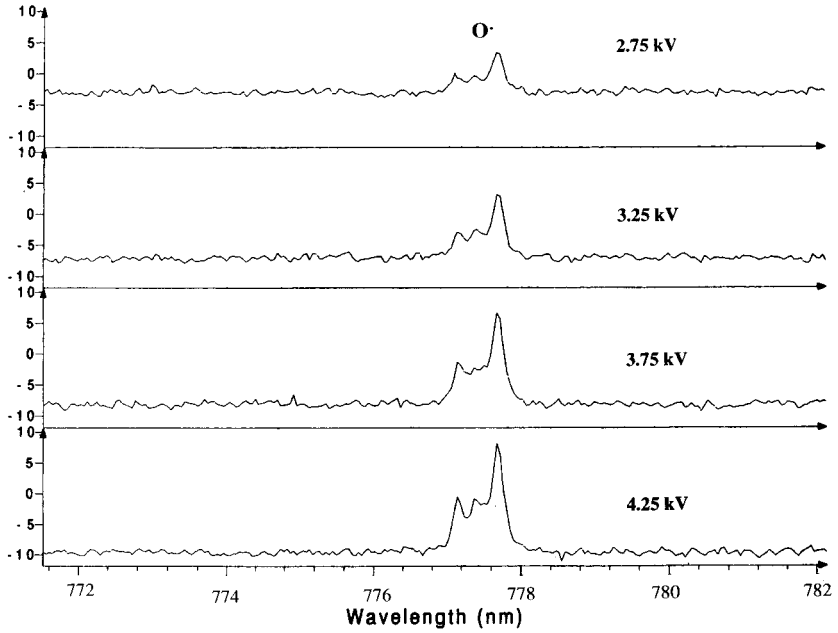

Figure 15. Spectra of oxygen radicals at different input voltages (3.1% H_2O/He, 20 mL/min) with quartz reactors.

TABLE 1: Bonding Energy of Related Reactant Molecules and Energy of Emitting State of Excited Plasma Species over Ground State (Data Converted from kJ/mol to eV from Ref 44)

bond	bonding energy, eV
H−O	4.7
O═O	5.1
N≡O	6.3
N≡N	9.8

reactions for NO decomposition and water splitting are proposed as shown in eqs 5−8 and eqs 9−13, respectively.

$$NO + He^* \rightarrow NO^* \quad (5)$$

$$NO^* \rightarrow N^\bullet + O^\bullet \quad (6)$$

$$2N^\bullet \rightarrow N_2 \quad (7)$$

$$2O^\bullet \rightarrow O_2 \quad (8)$$

$$H_2O + He^* \rightarrow H_2O^* + He \quad (9)$$

$$H_2O^* \rightarrow H^\bullet + HO^\bullet \quad (10)$$

$$HO^\bullet + He^* \rightarrow H^\bullet + O^\bullet + He \quad (11)$$

$$2H^\bullet \rightarrow H_2 \quad (12)$$

$$2O^\bullet \rightarrow O_2 \quad (13)$$

where the starred species signify excited species. He* are the excited species of He^+, He_2^+, He_2, and He 3^3S. Other excited He atoms are inactive. For nitrogen plasmas, all excited species are almost equally effective in activating reactant molecules, so He* in eqs 5−13 has been substituted for N_2^*/N_2^{+*}. All excited species in argon plasmas are also active, although with different energy-transfer efficiencies.

Basic data such as bond energies of related reactant molecules and energies of emitting states of excited species of helium, argon, and nitrogen are listed in Tables 1 and 2. Excited helium species possess the highest energy for activation of gas molecules. Excited nitrogen molecules are less energetic. However, even the energy of excitation of nitrogen is much higher than the bonding energy of any of the gas molecules, showing that plasmas employed in this study are capable of exciting any of the reactant molecules. All excited nitrogen species in nitrogen plasmas including N_2^+ are equally effective in energy transfer to water molecules, although the excitation energies of N_2^+ species are much higher. In argon plasmas the efficiency for different states of argon atoms are somehow different, showing also selectivity in energy transfer. Excited helium species show the highest selectivity in energy transfer in this study, although de-excitation energies of all states of excited helium atoms, including the active He 3^3S species, are very close (Table 2). There is no clear simple relation between the energy of de-excitation of different states and their selectivities in energy transfer. At present we are not aware of the reason for the difference in selective energy-transfer features between different plasmas.

TABLE 2: Important Emission Lines Identified in Plasmas of Helium, Argon, and Nitrogen Neat and in the Presence of Air, NO, or H_2O (Identification and Symbols Based on Refs 29 and 41 and Energies Converted to eV from cm^{-1})

plasmas	wavelength (nm)	transition	energy of emitting state (eV)
helium	388.9	$3^3P^0 \rightarrow 2^3S$	23.01
	501.6	$3^1P^0 \rightarrow 2^1S$	23.09
	587.6	$3^3D \rightarrow 2^3P^0$	23.07
	667.8	$3^1D \rightarrow 2^1P^0$	23.07
	706.5	$3^3S \rightarrow 2^3P^0$	22.72
	728.1	$3^1S \rightarrow 2^1P^0$	22.92
argon	696.5	$4p'[1/2] \rightarrow 4s[1^1/_2]^0$	13.33
	750.4	$4p'[1/2] \rightarrow 4s'[1/2]^0$	13.48
	763.5	$4p[1^1/_2] \rightarrow 4s[1^1/_2]^0$	13.17
	772.4	$4p'[1/2] \rightarrow 4s'[1/2]^0$	13.33
	811.5	$4p[2^1/_2] \rightarrow 4s[1^1/_2]^0$	13.08
	842.5	$4p[2^1/_2] \rightarrow 4s[1^1/_2]^0$	13.09
nitrogen	337.1 (N_2 2nd pos)	$C^3\Pi_u \rightarrow B^3\Pi_g$	11.1
	391.4 (N_2^+ 1st neg)	$B^2\Sigma_u^+ \rightarrow X^2\Sigma_g^+$	18.7

The parameter of energy-transfer efficiency can be used to correlate the activity and energy efficiency in reactions with quartz reactors. At higher input voltages and, therefore, higher excitation temperatures, more excited species are populated at

higher energy levels. The intensities of emission lines increase with increasing input voltage for plasmas of pure carrier gases. The energy-transfer efficiency increases in the same manner when reactants are introduced. Accordingly, more reactant molecules can be activated, leading to a higher activity at higher input voltages or higher plasma power. The sequence of energy-transfer efficiency observed for different diluent gases is also in accord with the sequence of hydrogen yields and energy efficiency observed in water splitting with these plasmas. This explains that in quartz reactors the reaction energy efficiency is determined by the efficiency of energy transfer from excited plasma species to reactant molecules.

However, lower energy-transfer efficiency and lower temperatures of excitation but higher activities and higher reaction efficiencies were observed with metal reactors compared to quartz reactors. Although the efficiency of energy transfer increases with increasing input voltage, the energy efficiency of reactions decreases upon increasing input voltage. This is because the catalytic function of metal surfaces plays an important role in these reactions.

B. Interaction between Metal Surfaces and Plasma Species and Catalytic Mechanisms. *1. Heterogeneous Catalysis of Metal Surfaces Involved in Plasma-Induced Water Splitting.* In a quartz reactor, where interactions between quartz surfaces and $O^{\bullet}$ are not observed, plasma-induced reactions are gas-phase processes. For water splitting, the radicals ($H^{\bullet}$, $HO^{\bullet}$, $O^{\bullet}$) formed are in the plasma phase and are easily recombined into water molecules. The reactions such as $H_2O \rightarrow H^{\bullet} + HO^{\bullet}$ and $HO^{\bullet} \rightarrow O^{\bullet} + H^{\bullet}$ in a quartz reactor might be governed by thermodynamic equilibria. The yield of hydrogen is therefore very low for quartz reactors with respect to metal electrodes. This is consistent with the result that the concentration of intermediates ($HO^{\bullet}$, $O^{\bullet}$, and H_α) in water splitting with quartz reactors is independent of flow rate of reactant but increases with increasing input voltages.

In a Pt reactor, metal surfaces participate in reactions by adsorbing oxygen radicals. Adsorbed oxygen radicals are combined into O_2. Since GC analyses show no oxygen loss after the initial activity drop, the formed O_2 must desorb into the gas phase from metal surfaces. The equilibrium of water splitting is therefore shifted toward decomposition of H_2O and $HO^{\bullet}$, producing H_2 of much higher yields, higher than that predicted by thermodynamics. This explains the absence of $O^{\bullet}$ and much lower concentrations of $HO^{\bullet}$ and H_α with metal reactors with respect to quartz reactors. The adsorption/desorption steps and surface reactions constitute the heterogeneous processes that catalyze plasma-induced water splitting. The adsorption of oxygen radicals also explains the higher initial activities with considerable initial activity drop for fresh metal electrodes (steps a, c in Figure 16).

Adsorbed oxygen radicals may also migrate into the bulk of active metal electrodes and form bulk metal oxides (step b in Figure 16). Dielectric bulk oxides on active metals (Fe, Ni, Cu) may influence the reaction in different ways, leading to higher initial activity and also higher deactivation rates with respect to Pt reactors. Stable Pt electrodes are relatively resistant to oxygen species and therefore correspond to a relatively lower initial activity and smaller deactivation.

2. NO Decomposition. NO decomposition is thermodynamically spontaneous ($\Delta G < 0$). Once activated, NO is easily decomposed into the much more stable products N_2/O_2. High and stable activity for NO decomposition is achieved with quartz reactors for this reason. The activity enhancement of metal surfaces is less pronounced in NO decomposition than in water

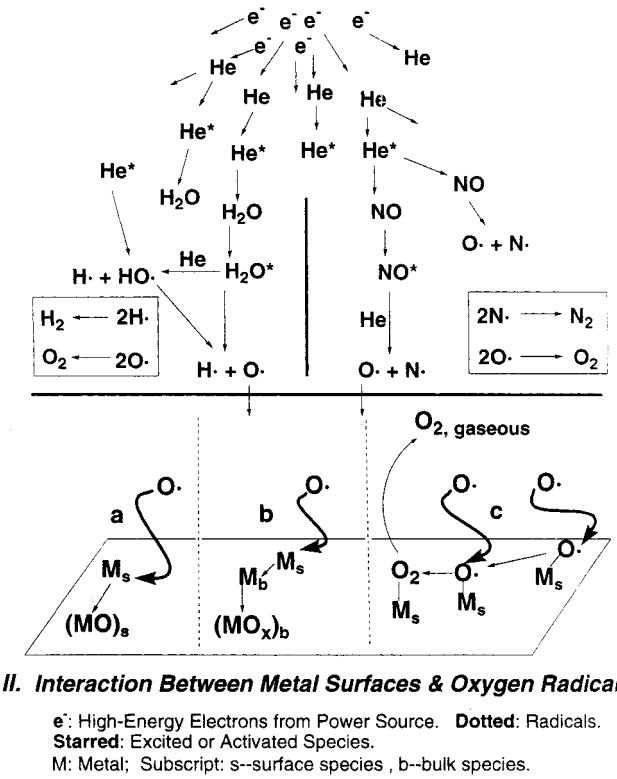

Figure 16. Mechanistic scheme showing interactions between excited carrier gas and reactant molecules and between plasma species and metal surfaces.

splitting. However, heterogeneous catalysis in plasma decomposition is due to adsorption/desorption on metal surfaces, as has been shown for different metal electrodes. In fact, differences in activity between quartz and metal reactors, and those among metal reactors, are obvious, which can also be explained by the strength and type of interactions between metal surfaces and $O^{\bullet}$ radicals.

V. Conclusions

Reactant molecules are activated via energy transfer from excited carrier gas species in plasma-induced reactions, where both plasma parameters (such as input voltages or power and excitation temperatures) and catalysis of metal surfaces play important roles. Energy transfer in helium plasmas is selective, in nitrogen plasmas is nonselective, and in argon plasmas is slightly selective. No heterogeneous catalysis has been observed for reactions with quartz reactors, where lower yet stable activity is obtained and the energy efficiency for reactions is determined by the efficiency for energy transfer from excited carrier gas species to reactant molecules. Heterogeneous catalysis of metal surfaces has been observed in reactions with metal electrodes, which comprises interactions between plasma species and metal surfaces. Oxygen radicals formed in the plasma-induced reactions are adsorbed on metal surfaces and quickly combine into O_2, thus shifting the equilibrium in the direction of water decomposition and NO decomposition. Surface metal oxides may be formed on fresh stable metal electrodes such as Pt, while both surface and bulk metal oxides can be formed on active metal electrodes (Fe, Ni, Cu). Therefore, a much higher activity with a marked initial activity drop followed by deactivation with different rates is associated with metal reactors.

Acknowledgment. The authors thank Dr. F. S. Galasso, Dr. Y. Yin, Dr. S. L. Brock, Mr. Xiandong Hou, and Ms. Qsun Sun for helpful discussions and assistance in experiments. Support for this research from Fujitsu Limited, Hokushin Corporation, and Honda R. and D. Co. is gratefully acknowledged.

References and Notes

(1) Evans, D.; Rosocha, L. A.; Anderson, G. K.; Coogan, J. J.; Kushner, M. J. *J. Appl. Phys.* **1993**, *74*, 5378−5386.

(2) Hsiao, M. C.; Merritt, B. T.; Penetrante, B. M.; Vogtlin, G. E.; Wallman, P. H. *J. Appl. Phys.* **1995**, *78*, 3451−3456.

(3) Futamura, S.; Yamamoto, T. *IEEE Trans. Ind. Appl.* **1997**, *33*, 447−453.

(4) Deng, G.; Zhang, Y.; Yu, Y.; Zou, D.; Hou, H.; Li, C. *J. Environ. Sci.* **1997**, *9*, 11−19.

(5) Penetrante, B. M.; Hsiao, M. C.; Bardsley, J. N.; Merritt, B. T.; Vogtlin, G. E.; Wallman, P. H.; Kuthi, A.; Burkhart, C. P.; Bayless, J. R. *Phys. Lett. A* **1995**, *209*, 69−77.

(6) Civitano, L.; Sani, E. In *Plasma Technology*; Capitelli, M., Gorse, C., Eds.; Plenum Press: New York, 1992; pp 153−166.

(7) Clements, J. S.; Mizuno, A.; Finney, W. C.; Davis, R. H. *IEEE Trans. Ind. Appl.* **1989**, *25*, 62−69.

(8) Fujii, K. In *Plasma Technology*; Capitelli, M., Gorse, C., Eds.; Plenum Press: New York, 1992; pp 143−152.

(9) Tas, M. A.; van Hardeveld, R.; van Veldhuizen, E. M. *Plasma Chem. Plasma Process.* **1997**, *17*, 371−391.

(10) Chang, M. B.; Balbach, J. H. *J. Appl. Phy.* **1991**, *69*, 4409−4417.

(11) Gallinberti, I. *Pure Appl. Chem.* **1988**, *60*, 663−674.

(12) Antonov, E. E.; Dresvyannikov, V. G.; Popovich, V. I. *J. New Energy* **1996**, *1*, 69−75.

(13) Lockwood, R. B.; Miers, R. E.; Anderson, L. W.; Lawler, J. E.; Lin, C. C. *Appl. Phys. Lett.* **1989**, *55*, 1385−1387.

(14) Badani, M. V.; Huang, J.; Suib, S. L.; Harrison, J. B.; Hahlauoi, M. *Res. Chem. Intermed.* **1995**, *21*, 621−630.

(15) Manukonda, R.; Dillon, R.; Furtak, T. *J. Vac. Sci. Technol. A* **1995**, *13*, 1150−1154.

(16) Gibalov, V. I.; Drimal, J.; Wronski, M.; Samoilovich, V. G. *Contrib. Plasma Phys.* **1991**, *31*, 89−99.

(17) Eremin, E. N.; Mat'tsev, A. N.; Syaduk, V. L. *Russ. J. Phys. Chem.* **1971,** *45*, 635−638.

(18) Huang, J.; Badani, M. V.; Suib, S. L.; Harrison, J. B.; Kablaoui, M. *J. Phys. Chem.* **1994**, *98*, 206−210.

(19) Huang, J.; Suib, S. L. *J. Phys. Chem.* **1993**, *97*, 9403−9407.

(20) Buser, R. G.; Sullivan, J. J. *J. Appl. Chem.* **1988**, *60*, 663−674.

(21) Eremin, E. N.; Mat'tsev, A. N.; Belova, V. M. *Russ. J. Phys. Chem.* **1965**, *43*, 443

(22) Luo, J.; Suib, S. L.; Marquez, M.; Hayashi, Y.; Matsumoto, H. *J. Phys. Chem. A* **1998**, *102*, 7954−7963.

(23) Suib, S. L.; Brock, S. L.; Marquez, M.; Luo, J.; Hayashi, Y.; Matsumoto, H. *J. Phys. Chem. B* **1998**, *102*, 9661−9666.

(24) Chen, X.; Marquez, M.; Rozak, J.; Murun, C.; Luo, J.; Suib, S. L.; Hayashi, Y.; Matsumoto, H. *J. Catal.* **1998**, *178*, 372−377.

(25) Brock, S. L.; Marquez, M.; Suib, S. L.; Hayashi, Y.; Matsumoto, H. *J. Catal.* **1998**, *180*, 225−233.

(26) Eremin, E. N.; Mal'tsev, A. N.; Belova, V. M. *Russ. J. Phys. Chem.* **1971**, *45*, 205−207.

(27) Volblikova, V. A.; Filippov, Y. V.; Vendillo, V. P. *Russ. J. Phys. Chem.* **1980**, *54*, 1416−1418.

(28) Tanaka, S.; Uyama, H.; Matsumoto, O. *Plasma Chem. Plasma Process.* **1994**, *14*, 491−504.

(29) Quintero, M. C.; Rodero, A.; Garcia, M. C.; Sola, A. *Appl. Spectrosc.* **1997**, *51*, 778−784.

(30) Hasegawa, T.; Umemoto, M.; Haraguchi, H.; Hsiech, C.; Montaser, A. In *Inductively Coupled Plasmas in Analytical Atomic Spectroscopy*; Montaser, A., Golightly, D. W., Eds.; VCH Publishers: New York, 1992; p 375.

(31) Dionghong, D.; Borgarello, E.; Grätzel, M. *J. Am. Chem. Soc.* **1981**, *103*, 4685−4690.

(32) *Chem. Eng. News* **1998**, February 16, 26.

(33) Hara, M.; Konda, T.; Komoda, M.; Ikeda, S.; Shinohara, K.; Tanaka, A. *J. Chem. Soc., Chem. Commun.* **1998**, 357−358.

(34) *Kirk-Othmer Encyclopedia of Chemical Technology*, 4th ed.; John Wiley and Sons: New York, 1991; Vol. 13, pp 867−874.

(35) . *CRC Handbook of Chemistry and Physics*, 75th ed.; Lide, D. R.; CRC Press: Boca Raton, FL, 1994; Section 10, pp 1−127.

(36) Pearse, R. W. B.; Gaydon, A. G. *The Identification of Molecular Spectra*; Chapman and Hall: New York, 1976.

(37) Hill, P. C. *Phys, Rev. A* **1991**, *43*, 2546−2549.

(38) Huffman, R. E.; Tanaka, Y.; Larrabee, J. C. *J. Opt. Soc. Am.* **1962**, *52*, 851−860.

(39) Sekiya, H.; Tsuji, M.; Nishimura, Y. *J. Chem. Phys.* **1987**, *87*, 325−330.

(40) Piper, L. G.; Gunndel, L.; Velazco, J. E.; Setser, D. W. *J. Chem. Phys.* **1975**, *62*, 3883−3889.

(41) Yu, O. S.; Yasuda, H. K. *Plasma Chem. Plasma Process.* **1998**, *18*, 461−485.

(42) Miyazaki, T.; Nagasaka, S.; Kamiya, Y. *J. Phys. Chem.* **1993**, *97*, 10715−10719.

(43) Anderson, L. C.; Xu, M.; Mooney, C. E.; Rosynek, M. P.; Lunsford, J. H. *J. Am. Chem. Soc.* **1993**, *115*, 6322−6326.

(44) *Inorganic Chemistry*, 3rd ed.; Huheey, J. E., Ed.; Harper & Row: New York, 1983; pp A32−A40.